Experimental Implementation and Validation of Dual Adaptive Control for Mobile Robots

Marvin K. Bugeja [*, 1] **Simon G. Fabri** [**]

Department of Systems and Control Engineering
University of Malta, Msida, MSD 2080, Malta
[*] *mkbuge@eng.um.edu.mt* [**] *sgfabr@eng.um.edu.mt*

Abstract: This paper presents experimental results which validate the use of a novel dual adaptive controller for mobile robots operating in the presence of dynamic uncertainty. The control scheme, recently proposed by the same authors, has so far been tested by simulations only. The presented results show, for the first time, the successful application of neural network dual adaptive control in a practical mobile robot scenario. In contrast to other adaptive controllers hitherto proposed for mobile robots, the dual adaptive approach employed in this scheme does not treat estimation and control as two separate tasks, but aims to strike a balance between the two at all times. This improves the overall performance. The implementation details of the robot designed for the purpose of this research are also presented in this paper.

Keywords: Adaptive control, Stochastic control, Neural control, Mobile robots

1. INTRODUCTION

There exists a vast number of contributions on control of wheeled mobile robots (WMRs) Kanayama et al. [1990], Canudas de Wit et al. [1993], Luca et al. [2001] which completely ignore the robot dynamics and rely on the assumption that the control inputs, usually motor voltages, instantaneously establish the desired wheel velocities. Other publications which explicitly account for the robot dynamics due to its mass, friction and inertia Fierro and Lewis [1995], Corradini and Orlando [2001], show that this leads to an improved control performance. On the other hand, as argued in Fierro and Lewis [1995], perfect knowledge of the robot dynamics is unavailable in practice. In addition these parameters can also vary over time due to loading, wear, and ground conditions. Inspired by these issues of dynamic model uncertainty, several robust and adaptive WMR controllers have been proposed over the last decade. These include: pre-trained neuro-controllers and robust sliding-mode methods Corradini and Orlando [2001], parametric adaptive schemes Wang and Tsai [2004], and also functional-adaptive controllers de Sousa et al. [2002], in which the uncertainty is not restricted to parametric terms but covers the dynamic functions themselves.

However, all these adaptive controllers rely on the heuristic certainty equivalence (HCE) assumption. This means that the estimated functions are used by the controller as if they were the true ones, thereby ignoring completely the inherent uncertainty of the estimations. When the uncertainty is large, for instance during startup or when the unknown functions are changing, HCE often leads to large tracking errors and excessive control actions, which can excite unmodelled dynamics or even lead to instability Åström and Wittenmark [1995]. In contrast, the dynamic controller employed in this paper is not based on the HCE assumption but accounts for the estimates' uncertainty in the control design. The uncertainty is characterized from a stochastic approach, more specifically the so-called *dual control* principle introduced by Fel'dbaum [1965]. A dual adaptive control law is designed with two aims in mind: (i) to ensure that the output tracks the desired reference signal, with due consideration given to the estimates' uncertainty; (ii) to excite the plant input sufficiently so as to accelerate the estimation process, thereby reducing quickly the uncertainty in future estimates. These two features are known as *caution* and *probing* respectively Fabri and Kadirkamanathan [2001], Filatov and Unbehauen [2004], Åström and Wittenmark [1995].

The main contribution of the work presented in this paper is twofold. Firstly, it presents a set of results which validate and compare the employed dual adaptive control scheme experimentally for the first time, after it was originally proposed in our previous publication Bugeja and Fabri [2007], which included simulation results only. Secondly, it outlines the practical implementation of this dual adaptive scheme on a mobile robot platform designed and built for the purpose of this research. Generally speaking, very few adaptive controllers have ever been implemented on a physical WMR, D'Amico et al. [2001], Wang and Tsai [2004], Dixon et al. [2001], and none of these address fully the uncertainty in the WMR dynamic functions nor take a dual adaptive control approach.

The rest of the paper is organized as follows. Section 2 develops the discrete-time dynamic model of the WMR. This is then used in the employed dual adaptive dynamic controller presented in Section 3. Section 4 outlines the experimental set-up and presents a set of experimental

[1] Work supported by the National Grant RTDI-2004-026

results validating the proposed scheme. This is followed by a brief conclusion in Section 5.

2. NONHOLONOMIC WMR MODEL

The differentially driven WMR considered in this work is depicted in Fig. 1. The passive wheels are ignored and the following notation is adopted throughout the article:

P_o: midpoint on the driving axle
P_c: centre of mass without wheels
d: distance from P_o to P_c
b: distance from each wheel to P_o
r: radius of each wheel
m_c: mass of the platform without wheels
m_w: mass of each wheel
I_c: angular mass of the platform about P_c
I_w: angular mass of wheel about its axle
I_m: angular mass of wheel about its diameter

The robot state vector is given by $\boldsymbol{q} \triangleq [x \;\; y \;\; \phi \;\; \theta_r \;\; \theta_l]^T$, where (x, y) is the Cartesian coordinate of P_o, ϕ is the robot's orientation with reference to the xy frame, and θ_r, θ_l are the angular displacements of the right and left driving wheels respectively. The *pose* of the robot refers to the three-dimensional vector $\boldsymbol{p} \triangleq [x \;\; y \;\; \phi]$.

2.1 Kinematic Model

Assuming that the wheels roll without slipping, the kinematic model of this WMR, detailed in Bugeja and Fabri [2007], is given by:

$$\dot{\boldsymbol{q}} = \boldsymbol{S}(\boldsymbol{q})\boldsymbol{\nu},$$

where the velocity $\boldsymbol{\nu} \triangleq [\nu_r \;\; \nu_l]^T \triangleq \left[\dot{\theta}_r \;\; \dot{\theta}_l\right]^T$, and

$$\boldsymbol{S} = \begin{bmatrix} \frac{r}{2}\cos\phi & \frac{r}{2}\cos\phi \\ \frac{r}{2}\sin\phi & \frac{r}{2}\sin\phi \\ \frac{r}{2b} & -\frac{r}{2b} \\ 1 & 0 \\ 0 & 1 \end{bmatrix}.$$

2.2 Dynamic Model

The WMR dynamic model, detailed in Bugeja and Fabri [2007], is given by:

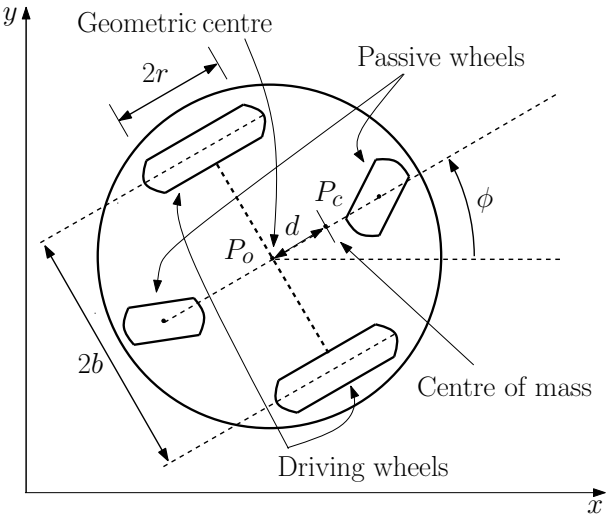

Fig. 1. Differentially driven wheeled mobile robot

$$\bar{\boldsymbol{M}}\dot{\boldsymbol{\nu}} + \bar{\boldsymbol{V}}(\dot{\boldsymbol{q}})\boldsymbol{\nu} + \bar{\boldsymbol{F}}(\dot{\boldsymbol{q}}) = \boldsymbol{\tau}, \tag{1}$$

where:

$$\bar{\boldsymbol{M}} = \begin{bmatrix} \frac{r^2}{4b^2}(mb^2 + I) + I_w & \frac{r^2}{4b^2}(mb^2 - I) \\ \frac{r^2}{4b^2}(mb^2 - I) & \frac{r^2}{4b^2}(mb^2 + I) + I_w \end{bmatrix},$$

$$\bar{\boldsymbol{V}}(\dot{\boldsymbol{q}}) = \begin{bmatrix} 0 & \frac{m_c r^2 d\dot{\phi}}{2b} \\ \frac{m_c r^2 d\dot{\phi}}{2b} & 0 \end{bmatrix}, \quad \bar{\boldsymbol{F}}(\dot{\boldsymbol{q}}) = \boldsymbol{S}^T(\boldsymbol{q})\boldsymbol{F}(\dot{\boldsymbol{q}}) \;,$$

$I = (I_c + m_c d^2) + 2(I_m + m_w b^2)$, $m = m_c + 2m_w$, $\boldsymbol{F}(\dot{\boldsymbol{q}})$ is a vector of frictional forces, $\boldsymbol{\tau} \triangleq [\tau_r \;\; \tau_l]^T$ with τ_r and τ_l being the torques applied at the right and left wheel respectively.

To account for the fact that the controller needs to be implemented on a digital computer, the continuous-time dynamics (1) are discretized through a first order forward Euler approximation with a sampling interval of T seconds, resulting in

$$\boldsymbol{\nu}_k - \boldsymbol{\nu}_{k-1} = \boldsymbol{f}_{k-1} + \boldsymbol{G}_{k-1}\boldsymbol{\tau}_{k-1}, \tag{2}$$

where subscript k denotes that the corresponding variable is evaluated at kT seconds, and vector $\boldsymbol{f}_{k-1}$ and matrix $\boldsymbol{G}_{k-1}$, which together encapsulate the WMR dynamics and in this work are assumed to be unknown to the controller, are given by

$$\begin{aligned} \boldsymbol{f}_{k-1} &= -T\bar{\boldsymbol{M}}_{k-1}^{-1}\left(\bar{\boldsymbol{V}}_{k-1}\boldsymbol{\nu}_{k-1} + \bar{\boldsymbol{F}}_{k-1}\right), \\ \boldsymbol{G}_{k-1} &= T\bar{\boldsymbol{M}}_{k-1}^{-1}. \end{aligned} \tag{3}$$

The following conditions are assumed to hold:

- The control input vector $\boldsymbol{\tau}$ remains constant over a sampling interval of T seconds.
- The sampling interval is chosen low enough for the approximation error to be negligible.

3. CONTROL SCHEME

The control aim is for the WMR to track a pre-specified trajectory in both pose and velocity in the presence of dynamic uncertainty. For this purpose, use is made of the trajectory-tracking dual adaptive dynamic control system by Bugeja and Fabri [2007] depicted in Fig. 2. Some variables in this figure are defined later in the article. At this point one should particularly note the modular architecture which enables the kinematic and dynamic control modules to be treated separately Fierro and Lewis [1995]. The task of the kinematic controller is to compute the desired wheel velocities in order to minimize the robot tracking error. The cascaded dynamic controller, which in the case of this paper is also *dual adaptive*, ensures that the robot truly tracks these velocities, by determining the torques required at the wheels.

3.1 Kinematic Control

To address the trajectory tracking problem we employ a discrete-time version of the kinematic controller originally proposed by Kanayama et al. [1990] and given by:

$$\boldsymbol{\nu_{ck}} = \boldsymbol{C}\begin{bmatrix} v_{rk}\cos e_{3k} + k_1 e_{1k} \\ \omega_{rk} + k_2 v_{rk} e_{2k} + k_3 v_{rk}\sin e_{3k} \end{bmatrix},$$

where $\boldsymbol{\nu_{ck}}$ is the computed wheel velocity command vector, k_1, k_2, and k_3 are *positive* design parameters, v_{rk} and

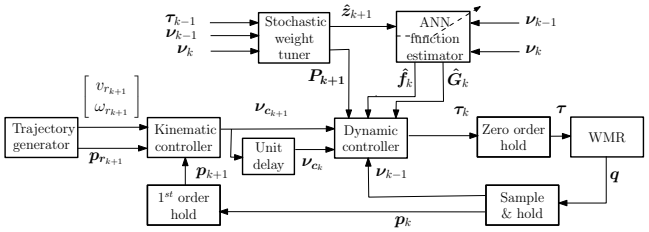

Fig. 2. Dual adaptive dynamic control scheme

ω_{rk} are the translational and angular *reference* velocities respectively (prespecified), $\boldsymbol{C}$ is a conversion matrix given by

$$\boldsymbol{C} = \begin{bmatrix} \frac{1}{r} & \frac{b}{r} \\ \frac{1}{r} & -\frac{b}{r} \end{bmatrix},$$

and e_{1k}, e_{2k}, e_{3k} constitute the tracking error

$$\boldsymbol{e}_k \triangleq \begin{bmatrix} e_{1k} \\ e_{2k} \\ e_{3k} \end{bmatrix} \triangleq \begin{bmatrix} \cos\phi_k & \sin\phi_k & 0 \\ -\sin\phi_k & \cos\phi_k & 0 \\ 0 & 0 & 1 \end{bmatrix} (\boldsymbol{p_r}_k - \boldsymbol{p}_k),$$

where $\boldsymbol{p_r}_k \triangleq [x_{rk} \;\; y_{rk} \;\; \phi_{rk}]^T$ denotes the reference pose vector at sampling instant k.

3.2 Dual Adaptive Dynamic Control

Neuro-Stochastic Estimator A three-layer radial basis function (RBF) ANN; composed of an input layer, a Gaussian hidden layer, and a linear output layer; is employed for the real-time estimation of the unknown vector of nonlinear functions $\boldsymbol{f}_{k-1}$, whose estimate is denoted by

$$\hat{\boldsymbol{f}}_{k-1} = \begin{bmatrix} \boldsymbol{\phi}^T(\boldsymbol{x}_{k-1})\hat{\boldsymbol{w}}_{\boldsymbol{1}k} \\ \boldsymbol{\phi}^T(\boldsymbol{x}_{k-1})\hat{\boldsymbol{w}}_{\boldsymbol{2}k} \end{bmatrix},$$

in the light of the following definitions: [2]

- $\boldsymbol{x}_{k-1}$, the ANN input vector, is set to $\boldsymbol{\nu}_{k-1}$.
- $\boldsymbol{\phi}(\boldsymbol{x})$ is the Gaussian RBF vector, whose ith element is given by

$$\phi_i = \exp\left(\frac{-(\boldsymbol{x}-\boldsymbol{m_i})^T \boldsymbol{R_r}^{-1}(\boldsymbol{x}-\boldsymbol{m_i})}{2}\right),$$

  where $\boldsymbol{m_i}$ is the centre-coordinate vector of the ith basis function, $\boldsymbol{R_r}$ is its spread, and time has been dropped for clarity.
- $\hat{\boldsymbol{w}}_{\boldsymbol{j}k}$ represents the synaptic weight vector of the connection between the basis functions and the jth output element of the network. The optimal weight vector $\boldsymbol{w}^*_{\boldsymbol{j}k}$ is unknown.
- L denotes the number of basis functions.
- $\boldsymbol{x}_{k-1}$ is assumed to be contained within an arbitrarily large compact set $\boldsymbol{\chi} \subset \mathbb{R}^2$.

Since $\boldsymbol{G}_{k-1}$, which is also unknown, is a symmetric state-independent matrix of parameters, its estimate does not require an ANN. Hence the estimate is simply denoted by

$$\hat{\boldsymbol{G}}_{k-1} = \begin{bmatrix} \hat{g}_{1k-1} & \hat{g}_{2k-1} \\ \hat{g}_{2k-1} & \hat{g}_{1k-1} \end{bmatrix},$$

where $\hat{g}_{1k-1}$ and $\hat{g}_{2k-1}$ are the estimates of unknown parameters in $\boldsymbol{G}_{k-1}$.

All the unknown optimal parameters and ANN weights requiring estimation are grouped in a vector given by $\boldsymbol{z}^*_k \triangleq [\boldsymbol{w}^{*T}_{\boldsymbol{1}k} \;\; \boldsymbol{w}^{*T}_{\boldsymbol{2}k} \;\; g^*_{1k-1} \;\; g^*_{2k-1}]^T$. In this work we treat this vector of unknowns as a random variable. Hence uncertainty is characterized in a stochastic sense. The WMR dynamic model (2) can thus be re-written in terms of $\boldsymbol{z}^*_k$ in the following state-space form:

$$\begin{aligned} \boldsymbol{z}^*_{k+1} &= \boldsymbol{z}^*_k \\ \boldsymbol{y}_k &= \boldsymbol{H}_{k-1}\boldsymbol{z}^*_k + \boldsymbol{\epsilon}_k \,, \end{aligned} \tag{4}$$

where the measured output $\boldsymbol{y}_k \triangleq \boldsymbol{\nu}_k - \boldsymbol{\nu}_{k-1}$, $\boldsymbol{\epsilon}_k$ is an independent zero-mean white Gaussian process with covariance $\boldsymbol{R_\epsilon}$, introduced to represent possible uncertainty in the measurements such as sensor noise, and $\boldsymbol{H}_{k-1} \triangleq [\boldsymbol{\Phi}_{k-1} \;\vdots\; \boldsymbol{\Gamma}_{k-1}]$ where

$$\boldsymbol{\Phi}_{k-1} \triangleq \begin{bmatrix} \boldsymbol{\phi}^T & \boldsymbol{0}^T \\ \boldsymbol{0}^T & \boldsymbol{\phi}^T \end{bmatrix}, \quad \boldsymbol{\Gamma}_{k-1} \triangleq \begin{bmatrix} \tau_{rk-1} & \tau_{lk-1} \\ \tau_{lk-1} & \tau_{rk-1} \end{bmatrix},$$

in which $\boldsymbol{0}$ is a zero vector bearing the same length as $\boldsymbol{\phi}$ and the time index in $\boldsymbol{\Phi}_{k-1}$ indicates that $\boldsymbol{\phi}$ is a function of $\boldsymbol{x}_{k-1}$.

Since (4) is linear in terms of the *random variable* requiring estimation $\boldsymbol{z}^*_k$, the Kalman filter in predictive mode is employed for the real-time least-square sense optimal stochastic estimation of $\boldsymbol{z}^*_{k+1}$, as shown below:

$$\begin{aligned} \hat{\boldsymbol{z}}_{k+1} &= \hat{\boldsymbol{z}}_k + \boldsymbol{K}_k \boldsymbol{i}_k \\ \boldsymbol{P}_{k+1} &= \boldsymbol{P}_k - \boldsymbol{K}_k \boldsymbol{H}_{k-1} \boldsymbol{P}_k, \end{aligned}$$

where $\boldsymbol{P}_k$ is estimate's covariance matrix, and the Kalman gain matrix and innovations vector are given by:
$\boldsymbol{K}_k = \boldsymbol{P}_k \boldsymbol{H}^T_{k-1} \left(\boldsymbol{H}_{k-1}\boldsymbol{P}_k\boldsymbol{H}^T_{k-1} + \boldsymbol{R_\epsilon}\right)^{-1}$ and
$\boldsymbol{i}_k = \boldsymbol{y}_k - \boldsymbol{H}_{k-1}\hat{\boldsymbol{z}}_k$ respectively.

Dual Adaptive Control Law The suboptimal dual adaptive dynamic control law employed in this work Bugeja and Fabri [2007] is given by

$$\begin{aligned} \boldsymbol{\tau}_k = &\left(\hat{\boldsymbol{G}}^T_k \boldsymbol{Q_1} \hat{\boldsymbol{G}}_k + \boldsymbol{Q_2} + \boldsymbol{N}_{k+1}\right)^{-1} \\ &\times \left(\hat{\boldsymbol{G}}^T_k \boldsymbol{Q_1}\left(\boldsymbol{y_d}_{k+1} - \hat{\boldsymbol{f}}_k\right) - \boldsymbol{\kappa}_{k+1}\right), \end{aligned} \tag{5}$$

where:

- $\boldsymbol{y_d}_{k+1}$ is the reference vector of $\boldsymbol{y}_{k+1}$ and is given by $\boldsymbol{y_d}_{k+1} \triangleq \boldsymbol{\nu_c}_{k+1} - \boldsymbol{\nu}_k$.
- Design parameters $\boldsymbol{Q_1}$, $\boldsymbol{Q_2}$ and $\boldsymbol{Q_3}$ are diagonal and $\in \mathbb{R}^{2\times 2}$. Additionally $\boldsymbol{Q_1}$ is positive definite, $\boldsymbol{Q_2}$ is positive semi-definite and each element of $\boldsymbol{Q_3}$ is ≤ 0 and $\geq$ the corresponding element of $-\boldsymbol{Q_1}$.

Let: (i) $\boldsymbol{Q_4} \triangleq \boldsymbol{Q_1} + \boldsymbol{Q_3}$, (ii) the i^{th} row j^{th} column element of any matrix $\boldsymbol{A_S}$ be denoted by $a_S(i,j)$, (iii) $\boldsymbol{P}_{k+1}$ to be repartitioned as

$$\boldsymbol{P}_{k+1} = \begin{bmatrix} \boldsymbol{P_{ff}}_{k+1} & \boldsymbol{P_{Gf}}^T_{k+1} \\ \boldsymbol{P_{Gf}}_{k+1} & \boldsymbol{P_{GG}}_{k+1} \end{bmatrix}$$

where $\boldsymbol{P_{ff}}_{k+1} \in \mathbb{R}^{2L_f \times 2L_f}$ and $\boldsymbol{P_{GG}}_{k+1} \in \mathbb{R}^{2\times 2}$, and (iv) auxiliary matrix $\boldsymbol{B} \triangleq \boldsymbol{P_{Gf}}_{k+1}\boldsymbol{\Phi}^T_k \boldsymbol{Q_4}$. Then:

- $\boldsymbol{\kappa}_{k+1} \triangleq \begin{bmatrix} b(1,1)+b(2,2) & b(1,2)+b(2,1) \end{bmatrix}^T$.
- The elements of $\boldsymbol{N}_{k+1}$ are given by:

[2] $\hat{}$ and * denote *estimate* and *optimal* values respectively.

$$
\begin{aligned}
n(1,1) &= q_4(1,1)p_{GG}(1,1) + q_4(2,2)p_{GG}(2,2) \\
n(2,2) &= q_4(1,1)p_{GG}(2,2) + q_4(2,2)p_{GG}(1,1) \\
n(1,2) &= \frac{1}{2}\Big(q_4(1,1)\big(p_{GG}(1,2) + p_{GG}(2,1)\big) \\
&\quad + q_4(2,2)\big(p_{GG}(1,2) + p_{GG}(2,1)\big)\Big) \\
n(2,1) &= n(1,2)\ .
\end{aligned}
$$

The time index in $\boldsymbol{N}_{k+1}$ indicates that each element $p_{GG}(\cdot,\cdot)$ corresponds to $\boldsymbol{P_{GG}}_{k+1}$.

The design parameter $\boldsymbol{Q_1}$ is introduced to penalize high deviations in the output and $\boldsymbol{Q_2}$ induces a penalty on large control signals and prevents ill-conditioning. $\boldsymbol{Q_3}$ affects the innovation vector so as to induce the *dual* feature characterizing our approach. It acts as a weighting factor where at one extreme, with $\boldsymbol{Q_3} = -\boldsymbol{Q_1}$, the controller completely ignores the estimates' uncertainty resulting in HCE control, and at the other extreme, with $\boldsymbol{Q_3} = \boldsymbol{0}$, it gives maximum attention to them, which leads to cautious control. For intermediate settings of $\boldsymbol{Q_3}$, the controller operates in a *dual adaptive* mode. It is well known that HCE control leads to large tracking errors and excessive control actions when the estimates' uncertainty is relatively high. On the other hand, cautious control is known for its slowness of response and *control turn-off*. Consequently, dual control exhibits superior performance by striking a balance between the two.

Fig. 3. NeuroBot: the experimental WMR

4. EXPERIMENTAL SET-UP AND RESULTS

The dual adaptive neuro-controller (5) was implemented successfully for the first time on a physical WMR, named NeuroBot, pictured in Fig. 3 which was designed and built by the authors as an experimental testbed.

NeuroBot is a differentially driven WMR. Each of the two 125mm diameter solid-rubber drive wheels, is independently driven by a 70W, 24V permanent magnet dc motor, which is equipped with a 113:1 reduction gearbox, and a 500 pulses per revolution incremental encoder. The effective number of encoder pulses had to be reduced electronically by a factor of eight. This was done in order to limit the extreme number of pulses interrupting the computing hardware (due to the high reduction ratio of the gearbox). Previously, this excessive number of encoder pulses was leading to erroneous speed measurements. The pulse division circuit implemented for this purpose, was designed specifically to retain the direction information encoded in the quadrature encoder signals.

Each of the two motors is driven via the LMD18200 H-Bridge IC which is controlled by a 20kHz pulse width modulation reference signal. The instantaneous current in each motor is measured using the LEM HX-03-P/SP2 Hall Effect current transducer, and filtered by a 4th-order continuous-time Bessel lowpass filter tuned for a corner frequency of 2kHz, and implemented using the MAX275 filter IC. NeuroBot is powered by four 12V, 9Ah sealed lead acid batteries.

The algorithms controlling NeuroBot are all implemented on a *MicroAutoBox* system from *dSPACE*. The *MicroAutoBox* is a compact stand-alone prototyping unit designed specifically for rapid-prototyping of computationally demanding real-time control systems, typically requiring a number of analog/digital input and output channels. A digital pole-placement torque controller with integral action was designed and implemented in software to account for the motor dynamics. This inner torque control loop uses the motor current measurement as feedback and issues voltage commands to the motors. This ascertains that the actual torques at the wheels track those issued by the outer loop control law (5). This cascade approach imposes that the inner loop operates at a much faster rate than the outer loop. The sampling rates for the inner and outer loops where chosen to be 10kHz and 200Hz respectively.

A number of experimental results which validate the proposed dual adaptive neuro-control scheme are presented in Figure 4. Plots (a) to (e) correspond to a challenging trajectory tracking experiment to test the overall functionality of the adaptive controller in *dual adaptive* mode. Plots (f) to (j) correspond to a line trajectory test with disturbance, and serve to compare the *dual adaptive* controller with its *HCE* and *cautious* counterparts. The neuro-adaptive controllers tested in this paper do not require any preliminary knowledge about the robot dynamics (3). Consequently the initial network parameter vector $\hat{\boldsymbol{z}}_0$ was generated randomly. The GaRBF ANN contained 25 basis functions with spread matrix $\boldsymbol{R_r} = 10\boldsymbol{I_2}$, where $\boldsymbol{I_i}$ denotes an $(i \times i)$ identity matrix.

Plot (a) depicts NeuroBot tracking a demanding reference trajectory with non-zero initial tracking error, when it

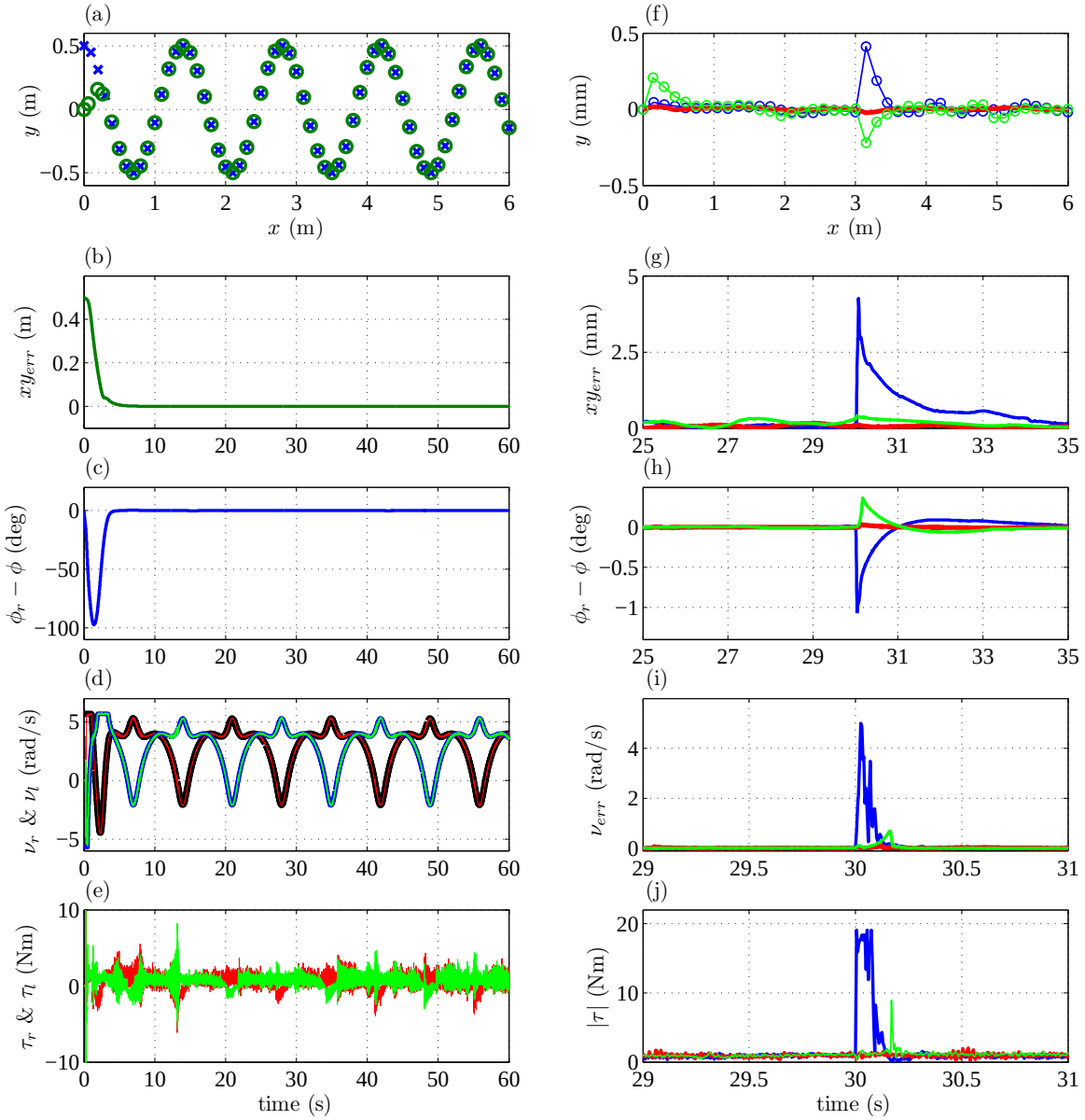

Fig. 4. (a): reference (blue) & actual (green) trajectories; (b): position error; (c): orientation error; (d): velocities - right (red), left (green) & their references (black & blue respectively); (e): torques - right (green), left (red); (f) to (j): comparative results - HCE (blue), Cautious (green), Dual (red).

is being controlled by the dual adaptive GaRBF scheme ($Q_3 = -0.8Q_1$). It is clear that NeuroBot swiftly adapts to its own dynamics and simultaneously converges smoothly to the reference trajectory. The WMR keeps tracking the trajectory with high precision for the rest of the experiment. Plots (b) and (c) show the position tracking error $xy_{err} \triangleq \sqrt{(}(x_r - x)^2 + (y_r - y)^2)$, and $\phi_r - \phi$ respectively. These plots clearly confirm that the trajectory tracking errors are all reduced to zero in a few seconds and remain there with unquestionable performance. Plot (d) shows the actual and reference angular wheel velocities along the trajectory. The actual velocities are practically superimposed on the corresponding references. This implies that the dual adaptive dynamic controller achieves the wheel velocities requested by the kinematic controller with great precision. Plot (e) depicts the wheel torques during this experiment, clearly implying that they remain well bounded for all time.

Plot (f) depicts the trajectories corresponding to the three adaptive controller modes (HCE, cautious and dual). In each case the reference trajectory is a constant velocity straight line on the x-axis, chosen specifically to facilitate comparative analysis. For evaluation purposes, in the middle of the trajectory (at $t = 30$s), the estimated parameter vector $\hat{\boldsymbol{z}}_{k+1}$ is instantaneously set to some arbitrary value, hence erasing all the knowledge acquired up to this point in time by the neuro-estimator. Consequently the covariance matrix $\boldsymbol{P}_{k+1}$ is set to a high value, reflecting the high uncertainty in the new set of arbitrary network parameters. In this manner one can objectively compare the transient performance of the three control modes when faced with

high uncertainty in the robot dynamics. This scenario is analogous to practical situations arising during faults and jump variations in the robot dynamics. The question in these cases is not simply whether or not the controller adapts to the new situation, but also how smoothly and quickly it will do so. Plots (f) to (j) clearly indicate that the dual controller exhibits the best transient performance among the other two controller modes. As anticipated in Section 1, HCE leads to large tracking errors (refer to Plots (f) to (i)) and excessive control actions (refer to Plot (j)), which can cause severe hardware failure if not limited properly. On the other hand, cautious control leads to a slower learning which also hinders the tracking performance. In fact we encountered situations where cautious control lead to *control turn-off*. In such cases the controller is so wary that the robot literally ceases to move altogether.

5. CONCLUSION

In this paper the dual adaptive dynamic control scheme, originally proposed by the authors in Bugeja and Fabri [2007], was validated experimentally for the first time. Moreover, the recently designed robotic testbed NeuroBot was introduced, and the associated implementation issues were briefly discussed. The experimental results presented in this paper not only validate the employed dual adaptive control scheme functional in practice, but clearly reveal the substantial improvements obtained in situations characterized by uncertainty and/or time-varying dynamics.

REFERENCES

K. J. Åström and B. Wittenmark. *Adaptive Control*. Addison-Wesley, Reading, MA, 2nd edition, 1995.

M. K. Bugeja and S. G. Fabri. Dual adaptive control for trajectory tracking of mobile robots. In *Proc. IEEE International Conference on Robotics and Automation (ICRA'07)*, pages 2215–2220, Rome, Italy, 2007.

C. Canudas de Wit, H. Khennoul, C. Samson, and O. J. Sordalen. Nonlinear control design for mobile robots. In Yuan F Zheng, editor, *Recent Trends in Mobile Robots*, Robotics and Automated Systems, chapter 5, pages 121–156. World Scientific, 1993.

M. L. Corradini and G. Orlando. Robust tracking control of mobile robots in the presence of uncertainties in the dynamic model. *Journal of Robotic Systems*, 18(6):317–323, 2001.

A. D'Amico, G. Ippoliti, and S. Longhi. A radial basis function networks apporach for the tracking problem of mobile robots. In *Proc. IEEE/ASME International Conference on Advanced Intelligent Mechatronics*, pages 498–503, Como, Italy, 2001.

C. de Sousa, E. M. Hemerly, and R. K. H. Galvao. Adaptive control for mobile robot using wavelet networks. *IEEE Trans. Syst., Man, Cybern.*, 32(4):493–504, 2002.

W. E. Dixon, D. M. Dawson, E. Zergeroglu, and A. Behal. Adaptive tracking control of a wheeled mobile robot via an uncalibrated camera system. *IEEE Trans. Syst., Man, Cybern. B*, 31(3):341–352, 2001.

S. G. Fabri and V. Kadirkamanathan. *Functional Adaptive Control: An Intelligent Systems Approach*. Springer-Verlag, London, UK, 2001.

A. A. Fel'dbaum. *Optimal Control Systems*. Academic Press, New York, NY, 1965.

R. Fierro and F. L. Lewis. Control of a nonholonomic mobile robot: Backstepping kinematics into dynamics. In *Proc. IEEE 34th Conference on Decision and Control (CDC'95)*, pages 3805–3810, New Orleans, LA, December 1995.

N. M. Filatov and H. Unbehauen. *Adaptive Dual Control: Theory and Applications*. Springer-Verlag, London, UK, 2004.

Y. Kanayama, Y. Kimura, F. Miyazaki, and T. Noguchi. A stable tracking control method for an autonomous mobile robot. In *Proc. IEEE Int. Conference of Robotics and Automation*, pages 384–389, Cincinnati, OH, May 1990.

A. De Luca, G. Oriolo, and M. Vendittelli. Control of wheeled mobile robots: An experimental overview. In S. Nicosia, B. Siciliano, A. Bicchi, and P. Valigi, editors, *RAMSETE - Articulated and Mobile Robotics for Services and Technologies*, volume 270 of *Lecture Notes in Control and Information Sciences*, pages 181–223. Springer-Verlag, 2001.

Tai-Yu Wang and Ching-Chih Tsai. Adaptive trajectory tracking control of a wheeled mobile robot via lyapunov techniques. In *Proc. 30th Annual Conference of the IEEE Industrial Electronics Society*, pages 389–394, Busan, Korea, November 2004.